

3D ultrasound-CT registration of the liver using combined landmark-intensity information

Thomas Lange · Nils Papenberg · Stefan Heldmann · Jan Modersitzki · Bernd Fischer · Hans Lamecker · Peter M. Schlag

Received: 10 January 2008 / Accepted: 23 September 2008 / Published online: 19 October 2008
© CARS 2008

Abstract

Purpose An important issue in computer-assisted surgery of the liver is a fast and reliable transfer of preoperative resection plans to the intraoperative situation. One problem is to match the planning data, derived from preoperative CT or MR images, with 3D ultrasound images of the liver, acquired during surgery. As the liver deforms significantly in the intraoperative situation non-rigid registration is necessary. This is a particularly challenging task because pre- and intraoperative image data stem from different modalities and ultrasound images are generally very noisy.

Methods One way to overcome these problems is to incorporate prior knowledge into the registration process. We propose a method of combining anatomical landmark information with a fast non-parametric intensity registration approach. Mathematically, this leads to a constrained optimization problem. As distance measure we use the normalized gradient field which allows for multimodal image registration.

Results A qualitative and quantitative validation on clinical liver data sets of three different patients has been performed. We used the distance of dense corresponding points on vessel center lines for quantitative validation. The combined landmark and intensity approach improves the mean and percentage of point distances above 3 mm compared to rigid and thin-plate spline registration based only on landmarks.

Conclusion The proposed algorithm offers the possibility to incorporate additional a priori knowledge—in terms of few landmarks—provided by a human expert into a non-rigid registration process.

Introduction

Accurate safety margins are essential for a beneficial long-term outcome in cases of liver tumor resections [1,2]. However, with increasing resection volume and less liver remnant morbidity rates as well as other risks to the patient are rising [3–6]. Therefore, it is extremely important to balance operative aggressiveness and optimal parenchyma preservation [7]. With modern computed tomography (CT) and magnetic resonance imaging (MRI) the individual anatomy and the location of the tumor in relation to vascular structures can be imaged with good accuracy. From such images, 3D models of the relevant structures and individual vascular territories can be computed [8], which are the basis of modern planning systems for liver surgery. These systems offer surgeons the possibility to perform detailed risk analysis and to define optimal individual resection plans [9] (Fig. 1a).

The challenging task is to transfer the preoperative plan precisely and securely to the intraoperative situation. The location of the tumor and relevant vessels is hidden underneath the liver surface and the correct location of the resection line can only be estimated. Intraoperative navigation systems support the surgeon by visualizing the spatial relation of surgical instruments with respect to invisible anatomical structures. Conventional navigation systems based only on preoperative data are not suitable for liver surgery, because the liver significantly deforms between preoperative imaging and the surgical procedure. Thus, dedicated navigation systems are based on either intraoperative liver surface

T. Lange (✉) · P. M. Schlag
Charité Comprehensive Cancer Center, Charité,
Universitätsmedizin Berlin, Berlin, Germany
e-mail: thomas.lange@charite.de

N. Papenberg · S. Heldmann · J. Modersitzki · B. Fischer
Institute of Mathematics, University of Lübeck, Lübeck, Germany

H. Lamecker
Zuse Institute Berlin, Berlin, Germany

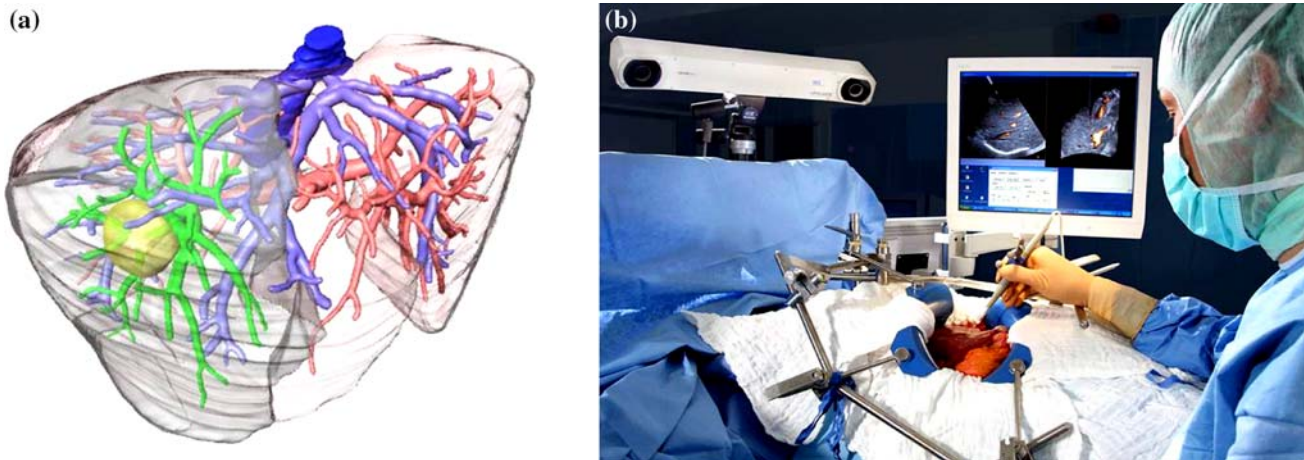


Fig. 1 a 3D liver resection plan with tumor (yellow) and vessels which have to be resected (green). The dark gray part of the liver tissue is supplied by the green part of the vessel tree and has to be resected.

b 3D ultrasound navigation system with Polaris localizer camera, tracked surgical instrument and navigation screen

information acquired by range scanners [10] or intraoperative 2D [11] or 3D ultrasound [12, 13] (Fig. 1b). Range scanners only capture the frontal part of the liver surface, yet significant features are rare on the surface. Furthermore, it is not clear how well liver deformations in the depth can be detected. This impedes the use of range scanners for registration purposes. By contrast, 3D ultrasound directly recovers volumetric regions, including tumors and important vessels.

Due to the mentioned deformations of the liver a reliable non-rigid registration algorithm is needed to transfer the preoperative plan to the intraoperative 3D ultrasound data. There is only few work published regarding CT/MR-ultrasound registration. Rigid methods have been presented, which are either intensity [14, 15] or feature-based [16, 17]. Usually the liver vessels serve as features, because of their easy identification in CT/MRI and ultrasound data, in particular in Power Doppler ultrasound. Extensions of such vessel-based approaches to non-rigid transformations are described in [18–21]. These methods, however, suffer from the problem that vessels cannot be extracted automatically from ultrasound data at high accuracy and speed. Alternatively, hybrid approaches [22] fit preoperatively extracted features directly to the intraoperative image data. In liver surgery those features are already available from surgery planning. An extension of these hybrid methods to non-rigid transformations is part of ongoing research [23].

A promising general approach is to incorporate a priori knowledge into the registration process. A priori knowledge induces constraints on the registration problem. Applying constraints reduces the level of non-uniqueness of a registration task and thus generates more reliable transformations. Using constraints is a very recent topic in image registration [24, 25].

One possibility for constraints are user-defined corresponding landmark pairs. Pure non-rigid landmark registration has already been applied to MRI-ultrasound registration [26]. Usually thin-plate splines (TPS) [27–29] are used as transformations of non-rigid landmark registration, but promising advancements have been published: elastic body splines (EBS) [30] and Gaussian elastic body splines (GEBS) [31]. In addition, anisotropic localization uncertainties have been considered leading to approximating TPS [32] or GEBS [33].

Nevertheless, registration based on landmarks alone ignores all the valuable information available from the image data. A combination of landmarks and image data leads to reliable registration strategies. Landmarks can be incorporated into a non-parametric intensity-based registration approach [29] either by adding a term to the registration functional which penalizes distances between corresponding landmarks (soft constraints) [34] or by formulating a constrained optimization problem (hard constraints) [35, 36].

We present a combined landmark-intensity registration method by formulating a constraint optimization problem like in [35]. In contrast to [35] a multi-modality distance measure is used and a completely different numerical scheme is introduced, which allows the application to clinical CT and 3D ultrasound data of patients who underwent oncological liver surgery.

Non-rigid registration

Thin plate spline registration

A common non-rigid registration approach based on landmarks alone is TPS warping. Since we will compare our

method, which is outlined in Sect. “Combined landmark and intensity registration”, to TPS warping we will briefly review it here.

Given N landmarks $r_j \in \mathbb{R}^3$ in an image $R : \Omega_R \rightarrow \mathbb{R}$ and corresponding landmarks $t_j \in \mathbb{R}^3$ in an image $T : \Omega_T \rightarrow \mathbb{R}$, where $\Omega_R, \Omega_T \subset \mathbb{R}^3$, TPS warping computes a smooth deformation field $y^{\text{TPS}} : \Omega_R \rightarrow \Omega_T$, which matches the landmarks, i.e., $y^{\text{TPS}}(r_j) = t_j$. The deformed template image T' is computed by evaluating $T \circ y^{\text{TPS}}$ for all $x \in \Omega_R$.

As mentioned before, TPS warping only takes into account landmarks but ignores image intensity information. Therefore one cannot expect a good match in regions where no landmark information is available.

Combined landmark and intensity registration

We propose to combine landmark with image intensity information within the registration process in the following way. The goal is to estimate a deformation $y = (y_1, y_2, y_3) : \Omega \rightarrow \mathbb{R}^3$ by minimizing an energy functional based on the images subject to the landmark conditions. Using the notation of Sect. “Thin plate spline registration”, we compute a solution to the following continuous constrained minimization problem:

$$\begin{aligned} \min_y \quad & \mathcal{J}(y) = \mathcal{D}(R, T(y)) + \alpha \mathcal{S}(y - y_0) \\ \text{s.t.} \quad & \mathcal{C}_j(y) = y(r_j) - t_j = 0, \quad j = 1, \dots, N. \end{aligned} \tag{1}$$

Here, \mathcal{D} is a measure for the similarity of the reference image R and the deformed template image $T(y)$. As a distance-measure we use the normalized gradient field (NGF) [37] given by

$$\mathcal{D}^{\text{NGF}}(R, T) = \frac{1}{2} \int_{\Omega} \left(\frac{\langle \nabla R(x), \nabla T(x) \rangle}{\|\nabla R(x)\| \|\nabla T(x)\|} \right)^2 dx.$$

This measure focuses on the alignment of edges in the given images, ignoring the absolute intensity values. Due to the different modalities CT and US of the images, standard distance-measures as, e.g., sum of squared differences, are not applicable for the multimodal setting. The particular choice of NGF has already been demonstrated in [34]. The measure is well suited for Power-Doppler-US which produces images with high contrast that are specific to vessels.

The second term $\alpha \mathcal{S}$ in equation (1) serves as a regularizer by measuring the smoothness of the deformation [29, 38, 39]. The parameter $\alpha > 0$ weights similarity vs. regularity, while y_0 is some user-supplied pre-registration. As regularization we use the well-known elastic regularizer [40]:

$$\mathcal{S}^{\text{elas}}(y) = \frac{1}{2} \int_{\Omega} \sum_{l=1}^3 \mu \|\nabla y_l\|^2 + (\mu + \lambda) \text{div}^2 y dx.$$

Discretization and optimization

We use the Discretize-Optimize approach [24] to achieve a minimizer of (1). This means the continuous optimization problem (1) is discretized first and subsequently finite dimensional optimization techniques are applied to the discrete problem.

Each of the building blocks of the optimization problem has to be discretized: the distance measure \mathcal{D}^{NGF} , the regularizer $\mathcal{S}^{\text{elas}}$ and the landmark constraints \mathcal{C} . A detailed description of the discretization is beyond the scope of the paper and can be found elsewhere [24, 41, 42], but the main ideas are outlined here.

Although the original images are discrete we need a continuous image representation to determine intensity values at the transformed grid points. We use cubic smoothing B-splines [43] to approximate the noisy image data. The advantage of these smoothing splines is their differentiability.

As usual in image processing, we identify voxels with cell-centered grid points. The discrete deformation y^h is defined on this grid. In order to use efficient optimization methods all parts of the discrete optimization problem have to be differentiable. The usage of staggered grids allows for fast and stable numerical schemes, see [24].

The discretization of the distance measure \mathcal{D}^{NGF} is given in [37] and of the elastic regularizer $\mathcal{S}^{\text{elas}}$ in [24], so only the discretization of the constraint function is given here. The transformed positions $y(r_j)$ of the landmarks r_j are approximated by tri-linear interpolation of the discrete deformation y^h : $y(r_j) \approx c_j^T y^h$ with interpolation coefficients c_j . Collecting all these coefficients into the matrix C the discrete version of the constraint function is given by

$$c(y^h) = C y^h - t. \tag{2}$$

After discretization of all building blocks we get the discretized version of the registration problem (1):

$$\begin{aligned} \min_{y^h} \quad & J(y^h) = D(R, T(y^h)) + \alpha \mathcal{S}(y^h - y_0^h) \\ \text{s.t.} \quad & c(y^h) = C y^h - t = 0. \end{aligned} \tag{3}$$

The constrained optimization problem (3) may be solved with a standard method like the Sequential Quadratic Programming algorithm [44]. However, due to the linearity of the constraints, we are able to eliminate the constraints and reformulate problem (3) as an unconstrained minimization problem.

The main idea is decompose the displacement into a special part y_{spec} that fulfills the constraint function and a homogeneous part y_{hom} that fulfills $C y_{\text{hom}} = 0$. One possible specific solution is a TPS $y_{\text{spec}} = y^{\text{TPS}}$, which interpolates the landmarks. Thus y^{TPS} satisfies the landmark constraints. Furthermore, each homogeneous solution can be represented as a linear combination of a basis of the Null space of C .

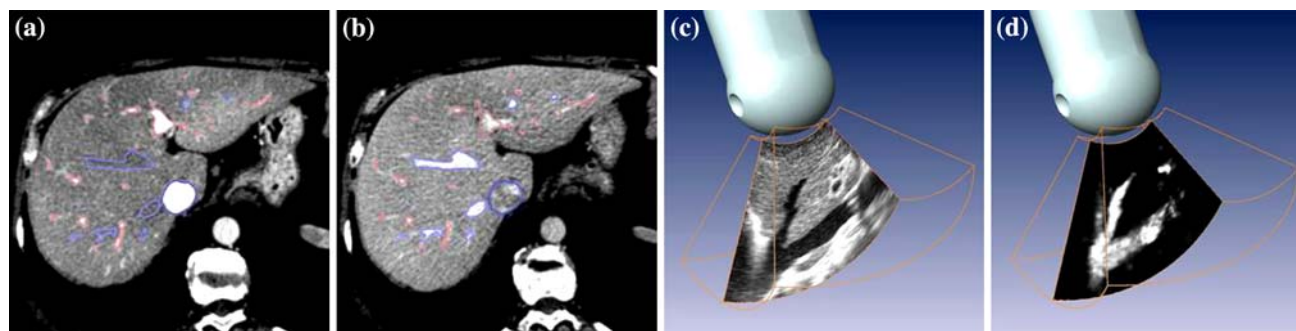


Fig. 2 **a** CT portal venous phase. **b** CT late venous phase. **c** B-Mode ultrasound. **d** Power Doppler ultrasound

Thus $y_{\text{hom}} = Zw$, with Z containing the bases vectors of the Null space of C and w the coefficient vector. Hence we get a parameterization of y in terms of the parameters w :

$$y(w) = y_{\text{hom}} + y_{\text{spec}} = Zw + y^{\text{TPS}}. \quad (4)$$

Henceforth, the optimization is performed via varying the parameters w and the resulting unconstrained optimization problem reads:

$$\begin{aligned} \min_w J(w) &= D(w) + \alpha S(w) \\ &= D(R, T(y(w))) + \alpha S(y(w) - y_0). \end{aligned}$$

For the solution of the unconstrained problem, we apply a standard Gauss–Newton scheme (like in [41]). Finally, to avoid local minima and to speedup convergence we also use a multi-level and multi-resolution approach via the parameter of the smoothing spline like in [41].

Specification of clinical image data

In this section, we describe the image data on which surgery planning and intraoperative navigation is based on.

CT data

For each patient a triphasic helical single-Source 64-Slice multidetector computed tomography (MDCT) scan of the abdomen (LightSpeed[®] VCT; General Electric Medical Systems, Milwaukee, WI) was acquired. The MDCT was performed after intravenous mechanical injection of 120 mL non-ionic iodinated contrast medium (iodine, 370 mg/mL; Ultravist[®] 370; Schering, Berlin, Germany) at a flow rate of 4 mL/s. Bolus tracking was used for an early arterial phase (upper abdomen) to optimize contrast filling of the vessels. This resulted in a scan delay of approximately 18 s. Delays of 20 and 60 s from the beginning of the early arterial scan were used for the portal venous (PV) (upper abdomen) and late venous phase (entire abdomen) scans, respectively. The collimation was set to 64×1.25 mm, with a gantry rotation time

of 0.7 s. The table feed was 13.75 mm/rotation for the arterial and PV phase and 35.0 mm/rotation for the venous phase. Tube current and voltage were set to 350 mA and 120 kV for the arterial and PV phase, and to 280 mA and 120 kV for the venous phase, respectively. Images were reconstructed with a slice thickness of 1.25 mm.

In the PV phase the hepatic veins are usually not enhanced (Fig. 2a). However, in the hepatic venous (HV) phase, portal veins are typically also visible, but with lower contrast as in the PV phase (Fig. 2b). PV as well as HV images are acquired during respiration hold, which is normally at end-inspiration. Due to patient respiration between acquisitions the position and shape of the liver sometimes cannot be reproduced exactly. So if information of portal and hepatic veins from different phases is to be used, the phases have to be registered [45]. In this paper we make use of the PV phase only.

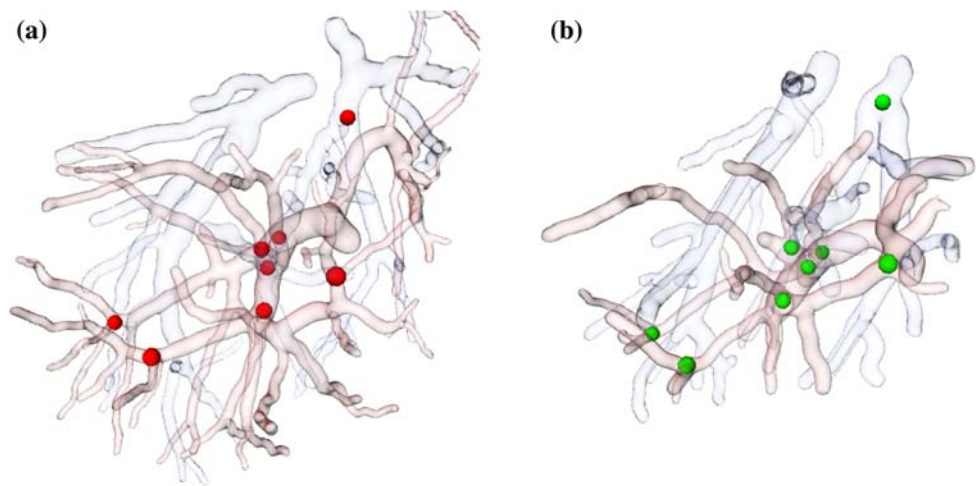
3D ultrasound

Different technologies for 3D ultrasound exist: (a) 3D ultrasound probes consisting of 2D arrays, (b) 2D tracked probes also called freehand 3D ultrasound and (c) 3D probes steered mechanically or electronically. The Voluson 730 ultrasound machine (GE Healthcare, Milwaukee, WI, USA) uses the latter technology: a 2D transducer is swept by a motor contained in a specific 3D ultrasound probe. The abdominal 3D transducer has a curved array, such that the swept volume is a part of a torus, because the radii of the sector in the image plane and the movement of the image plane may differ. Hence, the original image geometry is given in torus coordinates. The original data are transferred to the navigation computer via DICOM and reformatted to 0.5 mm isotropic voxels. B-mode and a Power Doppler ultrasound images are acquired synchronously (Fig. 2c, d). Thus both ultrasound modalities are naturally registered.

Landmark identification

Only a small number (usually 5–6, rarely up to 10) of corresponding point landmarks can be interactively identified in the

Fig. 3 Selected corresponding landmarks at vessel branchings from **a** CT data and **b** ultrasound data



available time window in the OR. Thus, efficient and intuitive interaction mechanisms are required to support landmark placement. For contrast-enhanced CT and Powerdoppler ultrasound images of the liver corresponding vessel branchings are a natural choice for point landmarks. In the preoperative CT data all branching points are computed in advance, based on the center lines of the segmented vessels. In order to interactively select a point landmark in CT data, the vessels are visualized as surfaces. When the user clicks on the surface near a vessel branching, then the nearest predetermined branching point is chosen automatically.

Unfortunately, reliable vessel segmentation from US images has not been achieved in a robust and accurate fashion, yet. Therefore, landmarks in the intraoperative US data have to be identified interactively in the intensity data. One way to improve the definition of the intraoperative landmarks is to click only approximately near the corresponding vessel branching and then automatically fit a vessel branching model to the intensity data at this location. This, however, is subject to future endeavors.

Results

The algorithm was validated on clinical image data pairs of three different patients. For each patient a computer assisted liver resection was performed. The preoperative planning and intraoperative navigation was based on the data described in the previous section. Only the PV phase of the preoperative CTs was used for registration. The portal veins are of high contrast in all cases, but the hepatic veins were hardly visible in cases 1 and 3 and significantly lower in case 2 compared to the portal veins. From two different ultrasound volumes only the Powerdoppler images were considered. Eight landmarks at branching points of the portal veins were chosen interactively (Fig. 3) lasting 5–10 min.

In all three cases a rigid registration was performed first, in order to compare to the results of the non-rigid registration approaches. Next, the TPS registration was performed based on the 8 landmark pairs. Finally, the combined approach was applied starting with the TPS displacement vector field as a specific solution of the landmark constraints (see Sect. “Discretization and optimization”).

The combined approach started with a grid spacing for the displacement vector field of 6 mm and ended with a finest spacing of 3 mm and 32^3 grid points. The resulting displacement field was interpolated to the original resolution of 0.5 mm. The run time of the optimization was approximately 10 min on an Intel Core Duo processor, with 1.83 Ghz and 2 GB RAM using MATLAB 7.6. The algorithm has not yet been optimized for runtime.

The maximal landmark difference after combined registration is below 0.3 mm (reached for case 1). These differences are due to the linear interpolation of the displacements at the landmarks from the neighboring grid points with a grid spacing of 3 mm. At the same time the distance measure reduces by 73% compared to TPS registration.

In Fig. 4 three differently oriented image planes illustrate the performance of the combined landmark-intensity registration approach in comparison to a rigid transformation and a TPS warping based on the landmarks alone. It is clearly visible, that a rigid transformation is not satisfactory justifying a non-rigid method. The combined method improves the TPS warping.

Quantitative validation of non-rigid registration methods is still a challenging problem and some evaluation criteria exist [46,47]. We used dense corresponding points on center lines of portal and hepatic veins (see [47] for detailed information). The distribution of the distances on the center lines are visualized in Fig. 5. The statistics of the distances is summarized in Tables 1 and 2.

The mean distances between corresponding points after rigid registration are in the range of 4.4–4.7 mm and 75–82%

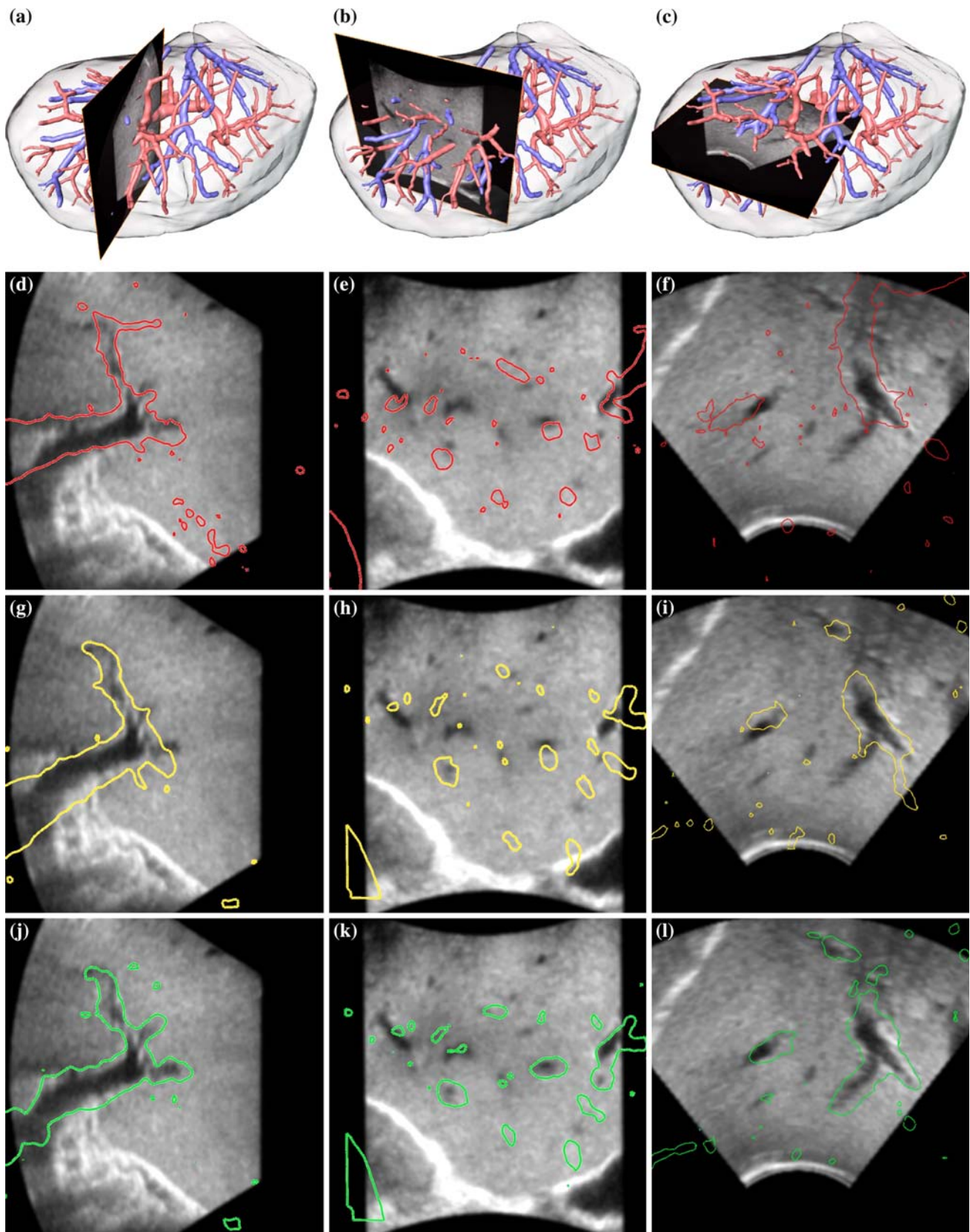


Fig. 4 Registration results for case 1. *First row*: Position of three different slice orientations in relation to liver model from CT data. The *second, third and fourth row* illustrate the transformed CT data as iso-

lines in the B-Mode ultrasound data. *Second row*: After rigid registration. *Third row*: After thin-plate spline registration. *Fourth row*: After combined non-linear landmark-intensity registration

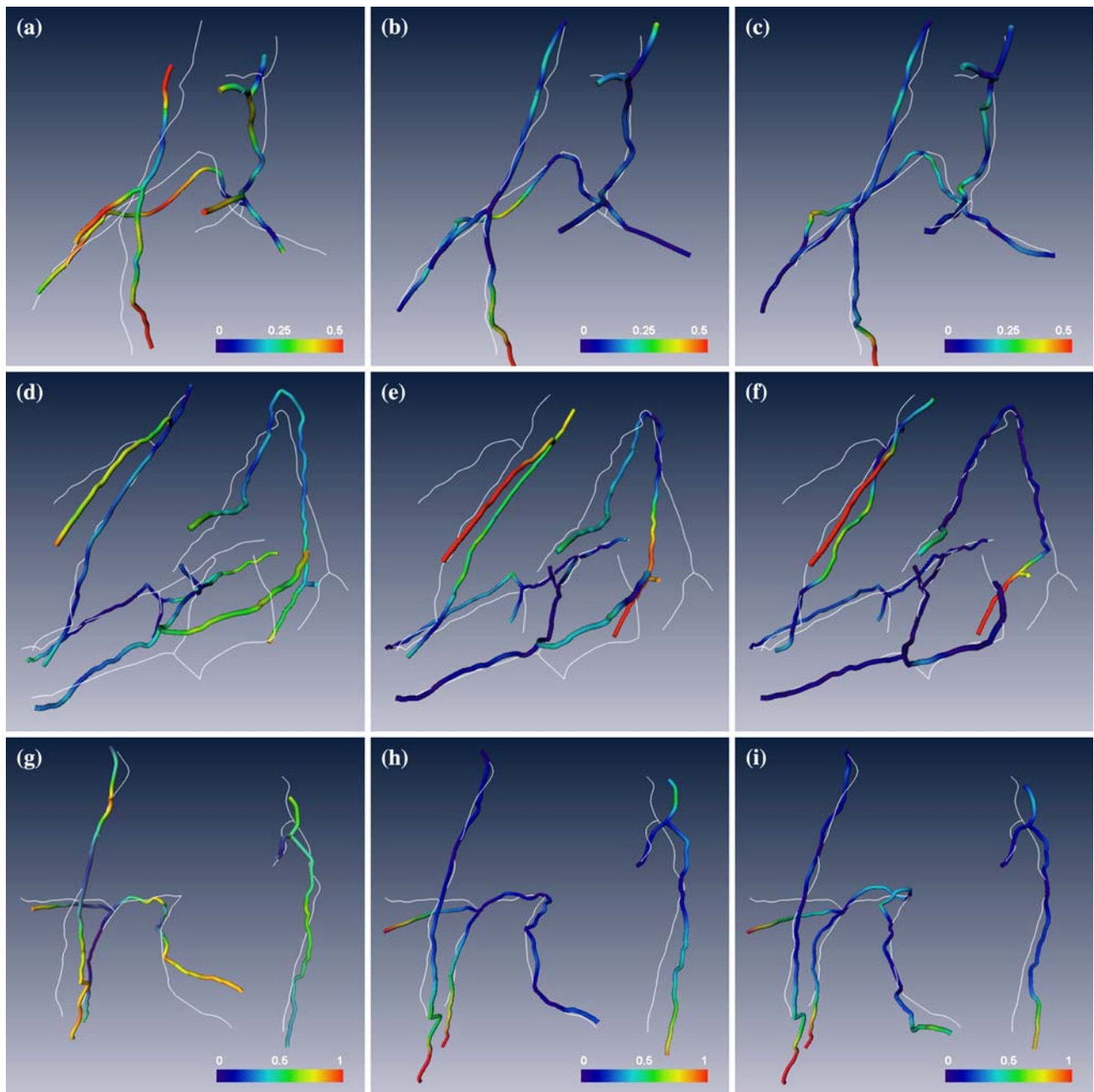


Fig. 5 Distribution of distances for corresponding points on vessel center lines. The distances are color-coded onto the registered model center lines. The *thin white lines* represent the reference center lines.

of the points are above 3 mm. This means there are significant deformations left after rigid registration. For case 1, TPS as well as the combined method reduce the distances considerably, but there is virtually no difference between TPS and combined method. In this case, however, the TPS registration already leads to good results. There is only small space left for improvements in this case. For case 2, TPS only slightly improves upon the rigid registration, yet the combined method improves significantly. For case 3, TPS and

Each row illustrates one clinical case. The *first column* shows the distributions after rigid, the *second column* after TPS and the *last column* after combined registration

combined method do not improve the rigid registration if looking at the mean distance, but the ratio of distances above 3 mm reduces, for the combined method more as for the TPS. Looking at the visualizations of the distances some vessel parts are very close (below 1 mm) after combined registration although the registration is based on the intensity images and not on the center lines. In case 2, there exist two parts of the hepatic veins, whose distance is high after rigid registration and still increases after TPS registration. It seems that the

Table 1 Mean (SD) distance between corresponding points on vessel center lines (mm)

	Rigid	TPS	Combined
Case 1	4.4 (± 1.8)	2.5 (± 2.0)	2.6 (± 2.0)
Case 2	4.6 (± 1.9)	4.6 (± 3.4)	3.6 (± 3.4)
Case 3	4.7 (± 2.3)	5.1 (± 4.2)	4.9 (± 4.3)

Table 2 Ratio of corresponding points on vessel center lines above 3 mm distance (%)

	Rigid (%)	TPS (%)	Combined (%)
Case 1	82	27	30
Case 2	76	61	41
Case 3	75	59	54

combined approach cannot compensate the large deviations that exist after TPS warping or are even induced by it.

Discussion and conclusions

Non-rigid registration of clinical preoperative CT and intraoperative 3D ultrasound data is still an open problem. In this paper we present an approach, which is an important step towards accurate and reliable schemes for non-rigid registration in clinical applications.

The main difficulties in our specific application are the quality of the US data with low contrast, high noise and artifacts, like shadowing in B-Mode ultrasound or motion artifacts in Powerdoppler ultrasound. In addition, the contrast of the hepatic veins is low in the PV phase of the CTs, and the contrast of the portal veins is low in the hepatic venous phase.

In this paper we have applied a combined landmark-intensity registration approach to clinical image pairs of PV phase CT and 3D Powerdoppler ultrasound data. The advantage of the method is that a priori knowledge—provided in terms of few landmarks—guides the registration process, and reduces the number of local minima. In contrast to incorporating the landmarks via a penalizer term no additional parameter has to be tuned in this constrained optimization formulation. The landmarks are guaranteed to match each other for each landmark pair. In case of a penalizer, however, the sum of the landmark distances is minimized through a trade-off with the distance measure and the regularizer. Thus, the distances of single landmark pairs might still be high after registration.

The qualitative and quantitative validation results are promising, yet some challenges remain. The first challenge is the low—or often non-existing—contrast of hepatic veins in

the PV phase of the CTs. A possible solution is to generate high contrast intensity models containing portal and hepatic veins (see [23]). In a preliminary experiment we used such intensity models for cases 1 and 3. In both cases we got an improved mean distance (case 1: 2.5 (± 1.5) mm, case 3: 4.4 (± 3.9) mm).

A second challenge are inaccuracies in the localization of the landmarks. In the presented approach no landmark errors are assumed. This leads to distorted vessels in some regions, because the endpoints of the vessels are forced to the inaccurate landmark positions. Incorporating landmarks as soft constraints is not an adequate solution to this problem, because the distance of corresponding landmarks is minimized only globally and not locally, as mentioned above. A better solution may be the introduction of local tolerances.

The third challenge has been revealed in “Results” Sect. TPS might provide a bad starting value in regions far away from landmarks. The combined registration process might not be able to compensate the initial displacements in these regions. Other interpolating functions like GEBS ([31]) are promising alternatives.

For further development other distance measures for multimodal image registration such as mutual information might be considered. As all available data sets (CT portal venous, CT late venous, B-Mode ultrasound, Powerdoppler ultrasound) provide complementary information, a consideration of all sets might further improve the registration process.

From a methodological point of view the algorithm has a lot of potential for different clinical applications by offering the possibility to incorporate additional a priori knowledge provided by a human expert into a non-rigid registration process. This interaction may be considered a drawback, because it is time-consuming and user-dependent. However, for the integration into the intraoperative navigation system the interaction will be reduced to a minimum through additional image processing techniques and intuitive interaction techniques.

Fully automatic CT/MR to 3D US registration is still an open problem and only few papers have been published. In order to progress towards a better understanding of the associated problems as well as to provide intermediate clinical solutions, additional interaction can be helpful, as we have shown in this paper. Clinical validation of non-rigid registration is a challenging and application-specific problem in itself. In the case of liver surgery, a registration accuracy in the range of 3 mm with a manual interaction time of about 10 min is reasonable for clinical application.

References

1. Bakalagos E, Kim J, Young D et al (1998) Determinants of survival following hepatic resection for metastatic colorectal cancer. *World J Surg* 22:399–404

2. Fong Y, Fortner J, Sun R et al (1999) Clinical score for predicting recurrence after hepatic resection for metastatic colorectal cancer: analysis of 1001 consecutive cases. *Ann Surg* 230:309–318
3. Abdalla E, Barnett C, Doherty D et al (2002) Extended hepatectomy in patients with hepatobiliary malignancies with and without preoperative portal vein embolization. *Arch Surg* 137:675–680
4. Shirabe K, Shimada M, Gion T et al (1999) Postoperative liver failure after major hepatic resection for hepatocellular carcinoma in the modern era with special reference to remnant liver volume. *J Am Coll Surg* 188:304–309
5. Shoup M, Gonen M, D'Angelica M et al (2003) Volumetric analysis predicts hepatic dysfunction in patients undergoing major liver resection. *J Gastrointest Surg* 7:325–330
6. Vauthey J, Chaoui A, Do K et al (2000) Standardized measurement of the future liver remnant prior to extended liver resection: methodology and clinical associations. *Surgery* 127:512–519
7. Redaelli C, Wagner M, Krahenbuhl L et al (2002) Liver surgery in the era of tissue-preserving resections: early and late outcome in patients with primary and secondary hepatic tumors. *World J Surg* 26:1126–1132
8. Selle D, Preim B, Schenk A, Peitgen HO (2002) Analysis of vasculature for liver surgical planning. *IEEE Trans Med Imaging* 21(11):1344–1357
9. Lang H, Radtke A, Hindennach M, Schroeder T, Fruhauf NR, Malago M et al (2005) Impact of virtual tumor resection and computer-assisted risk analysis on operation planning and intraoperative strategy in major hepatic resection. *Arch Surg* 140(7):629–638
10. Cash DM, Miga MI, Glasgow SC, Dawant BM, Clements LW, Cao Z et al (2007) Concepts and Preliminary Data Toward the Realization of Image-guided Liver Surgery. *J Gastrointest Surg* 11(7):844–859
11. Birth M, Kleemann M, Hildebrand P, Bruch HP (2004) Intraoperative online navigation of dissection of the hepatic tissue—a new dimension in liver surgery. In: *CARS*, pp 770–774
12. Beller S, Hünerbein M, Eulenstein S, Lange T, Schlag P (2007) Feasibility of navigated resection of liver tumors using multiplanar visualization of intraoperative 3D ultrasound data. *Ann Surg* 246(2):288–294
13. Beller S, Hünerbein M, Lange T, Eulenstein S, Gebauer B, Schlag PM (2007) Image-guided surgery of liver metastases by 3D ultrasound-based optoelectronic navigation. *Brit J Surg* 94(7):866–875
14. Roche A, Pennec X, Malandain G, Ayache N (2001) Rigid registration of 3-D ultrasound with MR images: a new approach combining intensity and gradient information. *IEEE Trans Med Imaging* 20(10):1038–1049
15. Slomka PJ, Mandel J, Downey D, Fenster A (2001) Evaluation of voxel-based registration of 3-D power Doppler ultrasound and 3-D magnetic resonance angiographic images of carotid arteries. *Ultrasound Med Biol* 27(7):945–955
16. Porter BC, Rubens DJ, Strang JG, Smith J, Totterman S, Parker KJ (2001) Three-dimensional registration and fusion of ultrasound and MRI using major vessels as fiducial markers. *IEEE Trans Med Imaging* 20(4):354–359
17. Penney GP, Blackall JM, Hamady MS, Sabharwal T, Adam A, Hawkes DJ (2004) Registration of freehand 3D ultrasound and magnetic resonance liver images. *Med Image Anal* 8(1):81–91
18. Lange T, Eulenstein S, Hünerbein M, Schlag PM (2003) Vessel-based non-rigid registration of MR/CT and 3D ultrasound for navigation in liver surgery. *Comput Aided Surg* 8(5):228–240
19. Lange T, Eulenstein S, Hünerbein M, Lamecker H, Schlag P (2004) Augmenting intraoperative 3D ultrasound with preoperative models for navigation in liver surgery. In: Barillot C, Haynor D, Hellier P (eds) *Medical image computing and computer-assisted intervention. Lecture notes in computer science*, vol 3217. Springer, Berlin, pp 534–541
20. Reinertsen I, Lindseth F, Unsgaard G, Collins D (2007) Clinical validation of vessel-based registration for correction of brain-shift. *Med Image Anal* (in press)
21. Reinertsen I, Descoteaux M, Siddiqi K, Collins D (2007) Validation of vessel-based registration for correction of brain shift. *Med Image Anal* 11(4):374–388
22. Aylward SR, Jomier J, Weeks S, Bullitt E (2003) Registration and analysis of vascular images. *Int J Comput Vision* 55(2–3):123–138
23. Lange T, Lamecker H, Hünerbein M, Eulenstein S, Beller S, Schlag P (2007) A distance measure for non-rigid registration of geometrical models to intensity data. In: Lemke H et al (eds) *CARS*, vol 2 (Supp 1) of *International Journal of Computer Assisted Radiology and Surgery*. Springer, Berlin, pp 204–206
24. Haber E, Modersitzki J (2004) Numerical methods for volume preserving image registration. *Inverse Probl* 20:1621–1638
25. Modersitzki J (2007) Image registration with local rigidity constraints. In: *Bildverarbeitung für die Medizin*, pp 444–448
26. Gobbi D, Comeau R, Peters T (2000) Ultrasound/mri overlay with image warping for neurosurgery. In: *Medical Image Computing and Computer-Assisted Intervention (MICCAI)*. Springer, Berlin, pp 106–114
27. Bookstein FL (1989) Principal warps: thin-plate splines and the decomposition of deformations. *IEEE Trans Pattern Anal Mach Intell* 11(6):567–585
28. Rohr K (2001) *Landmark-based image analysis*. Springer, Berlin
29. Modersitzki J (2004) *Numerical methods for image registration*. Oxford University Press, Oxford
30. Davis MH, Khotanzad A, Flaming DP, Harms SE (1997) A physics-based coordinate transformation for 3-D image matching. *IEEE Trans Med Imaging* 16(3):317–328
31. Kohlrausch J, Rohr K, Stiehl HS (2005) A new class of elastic body splines for nonrigid registration of medical images. *J Math Imaging Vis* 23:253–280
32. Rohr K, Stiehl H, Sprengel R, Buzug T, Weese J, Kuhn M (2001) Landmark-based elastic registration using approximating thin-plate splines. *IEEE Trans Med Imag* 20(6):526–534
33. Wörz S, Rohr K (2006) Physics-based elastic image registration using splines and including landmark localization uncertainties. In: *MICCAI* (2), pp 678–685
34. Papenberg N, Lange T, Modersitzki J, Schlag PM, Fischer B (2008) Image registration for CT and intra-operative ultrasound data of the liver. In: *SPIE Medical imaging: visualization, image-guided procedures, and modeling*, vol 6918 (accepted)
35. Fischer B, Modersitzki J (2003) Combining landmarks and intensity driven registrations. In: *PAMM Proceedings in Applied Mathematics and Mechanics*, vol 3, pp 32–35
36. Fischer B, Modersitzki J (2003) Combination of automatic non-rigid and landmark based registration: the best of both worlds. In: Sonka M, Fitzpatrick J (eds) *Medical imaging 2003: image processing*. Proceedings of the SPIE 5032, vol 5032, pp 1037–1048
37. Haber E, Modersitzki J (2007) Intensity gradient based registration and fusion of multi-modal images. *Methods Inf Med* 46(3):292–299
38. Fischer B, Modersitzki J (2003) FLIRT: a flexible image registration toolbox. In: Gee J, Maintz J, Vannier M (eds) *2nd International Workshop on Biomedical Image Registration 2003*, vol 2717. Springer, Berlin, pp 261–270
39. Papenberg N, Schumacher H, Heldmann S, Wirtz S, Bommerheim S, Ens K et al (2007) A fast and flexible image registration toolbox—design and implementation of the general approach. *Bildverarbeitung für die Medizin 2007. Informatik Aktuell*, pp 106–110

40. Broit C (1981) Optimal registration of deformed images. Department of Computer and Information Science, University of Pennsylvania
41. Haber E, Modersitzki J (2006) A multilevel method for image registration. *SIAM J Sci Comput* 27(5):1594–1607
42. Modersitzki J (2008) FLIRT with rigidity—image registration with a local non-rigidity penalty. *Int J Comput Vis* 76(2):153–163
43. Wahba G (1990) Spline models for observational data. SIAM, Philadelphia
44. Nocedal J, Wright SJ (1999) Numerical optimization. Springer, Berlin
45. Lange T, Wenckebach T, Lamecker H, Seebass M, Hünerbein M, Eulenstein S et al (2005) Registration of different phases of contrast-enhanced CT/MRI data for computer-assisted liver surgery planning: Evaluation of state-of-the-art methods. *Int J Med Robot Comput Assist Surg* 1(3):6–20
46. Christensen G, Geng X, Kuhl J, Bruss J, Grabowski T, Pirwani I et al (2006) Introduction to the non-rigid image registration evaluation project (NIREP). In: WBIR. Lecture notes in computer science, vol 4057. Springer, Berlin, pp 128–135
47. Lange T, Lamecker H, Hünerbein M, Eulenstein S, Beller S, Schlag PM (2008) Validation metrics for non-rigid registration of medical images containing vessel trees. In: Bildverarbeitung für die Medizin (BVM), pp 82–86